Metal Films Prepared by Stepwise Assembly. 2. Construction and Characterization of Colloidal Au and Ag Multilayers

Michael D. Musick,† Christine D. Keating,† L. Andrew Lyon,† Steven L. Botsko,† David J. Peña,† William D. Holliway,† Todd M. McEvoy,‡ John N. Richardson,‡ and Michael J. Natan*,†

Department of Chemistry, The Pennsylvania State University, 152 Davey Lab, University Park, Pennsylvania 16802-6300, and Department of Chemistry, Shippensburg University, 1871 Old Main Drive, Shippensburg, Pennsylvania 17257-2299

Received November 9, 1999. Revised Manuscript Received June 5, 2000

This manuscript describes the stepwise, ligand-directed assembly, characterization, and prospective applications of three-dimensional Au and Ag nanoparticle, multlilayered films. Films were prepared by successive treatments of a Au nanoparticle monolayer with a bifunctional cross-linker and colloidal Au or Ag solutions. Changes in film electrical and optical properties are reported for a series of bifunctional cross-linkers of varying molecular lengths. Interestingly, these films exhibit Beer's law behavior despite the presence of strong interparticle optical coupling. Multilayer films with greater than six exposures to 2-mercaptoethylamine and Au colloid were highly conductive and resembled bulk Au in appearance. In contrast, films of similar particle coverage generated using a longer cross-linker (1,6-hexanedithiol) exhibited higher transmission in the near-infrared region and exhibited a reduced conductivity. Measurement of the multilayer morphology with atomic force microscopy , electrostatic force microscopy, and field emission scanning electron microscopy revealed a porous, discontinuous morphology composed of large, continuous regions of aggregated nanoparticles. This, in turn, results in a surface roughness contribution to surface plasmon scattering and surface-enhanced Raman scattering observed for Au, Au/Ag, and Ag colloid multilayers. Particulate multilayer films made using horseradish peroxidase as a cross-linker remained enzymatically active, even beneath three layers of colloidal Au. Multilayers could also be prepared on surfaces patterned by microcontact printing. These data show how Au colloid multilayers grown in solution are a viable alternative to evaporated metal films for a number of applications.

Introduction

Ensembles of nanoparticles display unique optical and electrical properties that are distinct from their respective bulk properties and from average measurements of collections of widely spaced particles. To a large extent, however, bulk material properties (i.e., catalytic, optical, and electrical properties and biocompatibility) are determined by nanoscale features. The ability to tune particle, size, shape, chemical composition, array geometry, and linking chemistries provides a flexible platform to manipulate material properties through rational design of the principal components (i.e., metal or semiconductor nanoparticles). Several recent reviews and books detail recent progress and awaiting challenges associated with nanostructure control.[1]

Materials composed from two-dimensional (2-D) and three-dimensional (3-D) ensembles of nanoparticles are becoming increasingly important in analytical and materials chemistries; indeed, practical applications in nanoelectronic and optoelectronic devices, chemical sensors, and catalysis seem imminent. For example, arrays of crystalline-modified polystyrene spheres[2] and suspended ensembles of ligand-coated metal nanoparticles[3] are finding use as vapor-phase molecular recognition sensors. Self-organized 2-D nanoparticle superlattices of latex spheres, CdS,[4] CdSe,[5] Au,[6] and Ag[7] structures, have been constructed and analyzed. Organized 3-D arrays of nanoparticles with inter- and intralayer

* To whom correspondence should be addressed via e-mail: natan@chem.psu.edu.

† The Pennsylvania State University.

‡ Shippensburg University.

(1) (a) Schmid, G.; Lifeng C. F.; *Adv. Mater*. **1998**, *10*, 515−526. (b) Martin, C. R.; Mitchell, D. T. *Anal. Chem*. **1998**, *70*, 322A−326A. (c) Heath, J. R.; Kuekes, P. J.; Snider, G. S.; Williams, S. R. *Science* **1998**, *280*, 1716−1720. (d) Bethell, D.; Schriffrin, D. J. *Nature* **1996**, *382*, 581−611.

(2) (a) Holtz, J. H.; Holtz, J. S.; Munro, C. H.; Asher, S. A. *Anal. Chem*. **1998**, *70*, 780−791. (b) Holtz, J. H.; Asher, S. A. *Nature* **1997**, *389*, 829−822.

(3) Wohitjen, H.; Snow, A. W. *Anal. Chem*. **1998**, *70*, 780−791.

(4) (a) Hu, K.; Brust, M.; Bard, A. *Chem. Mater*. **1998**, *10*, 1160−1165. (b) Alvarez, M. M.; Khoury, J. T.; Schaatt, T. G.; Shafigullin, M. N,; Vezmar, I.; Whetten, R. L. *J. Phys. Chem. B* **1997**, *101*, 3706. (c) Kotov, N. A.; Meldrum, F. C.; Wu, C.; Fendler, J. H. *J. Phys. Chem*. **1994**, *98*, 2735−2738.

(5) (a) Murray, C. B.; Kagan, C. R.; Bawendi, M. G. *Science* **1995**, *270*, 1335−1338. (b) Tolbert, S. H.; Herhold, A. B.; Johnson, C. S.; Alivisatos, A. P. *Phys. Rev. Lett*. **1994**, *73*, 3266−3269. (c) Cassagneau, T.; Mallouk, T. E.; Fendler, J. H. *J. Am. Chem. Soc*. **1998**, *120*, 7848−7859.

10.1021/cm990714c CCC: $19.00
Published on Web 09/09/2000

particle registry have been assembled from polystyrene,[8] Ag,[9] CdS,[5] and inorganic oxide nanoparticles.[10] However, with the exception of the inorganic oxides reported by Colvin and co-workers, and separately by Stein and co-workers,[10] no assemblies extend more than a few layers above the substrate and offer more than modest control over film thickness.

Multilayers of nanoparticles produced by alternate immersion into a bifunctional cross-linker and nanoparticle solutions produce random arrays of nanoparticles of controllable thickness. Particle spacing of films grown "stepwise" or "layer-by-layer" are determined by the molecular size of the cross-linker. In this fashion, assemblies of dithiol-linked Cu[11] and polyion-linked CdS[12] and SiO_2[13] have been characterized. Multilayers of thiol-capped Au nanoclusters were described separately by the Schiffrin[6e,14] and Murray[15] groups, and the optical, electrical, and electrochemical properties of thiol-linked 12-nm diameter Au colloids have been described by the Natan group.[16,17] Willner and co-workers have constructed an electrochemical sensor based on donor−acceptor chemistry where hydroquinone, a π-acceptor, is concentrated in the Au colloid multulayer by bipyridinium cyclophane, a π-donor used as "molecular glue".[18] Rao and co-workers characterized, by X-ray diffraction, superlattices formed via layer-by-layer deposition of Pt, CdS, and Au nanoparticles.[19] Likewise, nanoparticles have been encapsulated in sol−gel and aerogel matrixes for evaluation as nonlinear optical materials or prospective catalysts.[20] Other advances in nanoparticle assembly include the temperature-dependent assembly/disassembly of oligodeoxyribonucleotide−Au colloid conjugate networks[21] and the construction of one-dimensional (1-D) arrays of Au−poly(pyrrole) nanoparticle arrays via membrane pore template synthesis, potentially a unique method to construct single-electron devices from solution.[22]

Interest in 2-D metal nanoparticle arrays stems from several unique characteristics. (i) These arrays are easy to synthesize. Concentrated solutions of monodispersed Au nanoparticles from 2 to 100 nm in diameter are easily synthesized.[23] Metal nanoparticles readily adsorb onto appropriately derivatized surfaces. Typically, organosilanes,[17,24] hyperbranched polymers,[25] or alkylthiols[26] are used to generate arrays with random packing but with a reproducible overall coverage and with a reasonable distribution of interparticle spacing. (ii) Optical properties are a function of particle spacing, size, and composition,[27−29] easily tailored attributes. (iii) Particles have a high surface area, useful for applications in catalysis, electrochemistry, biomolecule conjugation, and surface-sensitive spectroscopies. In contrast to sol−gel or polymer encapsulation,[20] where the majority of the particle is coupled to the matrix and inaccessible to solution or gas-phase chemistry, only a small fraction of an individual particle is in contact with the

(6) Mayva, K. S.; Sastry, M. *Langmuir* **1999**, *15*, 1902−1904. (b) Lin, X. M.; Sorensen, C. M. *Chem. Mater.* **1999**, *11*, 198−202. (c) Burmeister, F.; Schafle, C.; Keilhofer, B. Bechinger, C.; Bonenerg, J.; Leiderer, P. *Adv. Mater.* **1996**, *10*, 495−497. (d) Andres, R. P.; Bielefeld, J. D.; Henderson, J. I.; Janes, D. B.; Kolagunata, V. R.; Kubiak, C. P.; Mahoney, W. J.; Osifchin, R. G. *Science* **1996**, *273*, 1690−1693. (d) Giersig, M.; Mulvaney, P. *J. Phys. Chem.* **1993**, *97*, 6334−6336. (e) Bethell, D.; Brust, M.; Schiffrin, D. J.; Kiely, C. *J. Electroanal. Chem.* **1996**, *409*, 137−143.11. (f) Schmitt, J.; Decher, G.; Dressick, W. J.; Brandow, S. L.; Geer, R. E.; Shashidhar, R.; Calvert, J. M. *Adv. Mater.* **1997**, *9*, 61−65. (g) Leibowitz, F. L.; Zheng, W. X.; Maye, M. M.; Zhong, C. J. *Anal. Chem.* **1999**, *71*, 5076−5083. (h) Burghard, M.; Philipp, G.; Roth, S.; von Klitzing, K.; Pugin, R.; Schmid, G. *Adv. Mater.* **1998**, *10*, 842−846. (i) Hanaoka, T.; Kormann, H. P.; Kroll, M.; Sawitowski, T.; Schmid, G. *Eur. J. Inorg. Chem.* **1998**, *6*, 807−812.

(7) (a) Harfenist, S. A.; Wang, Z. L.; Alvarez, M. M.; Vezmar, I.; Whetten, R. L. *J. Phys. Chem.* **1996**, *100*, 13904−13910. (b) Korgel, B. A.; Fitzmaurice, D. *Adv. Mater.* **1998**, *10*, 661−665. (c) Remacle, F.; Collier, C. P.; Markovich, G.; Heath, J. R.; Banin, U.; Levine, R. D. *J. Phy. Chem. B* **1998**, *102*, 7727−7734. (d) Chung, S.-W.; Markovich, G.; Heath, J. R. *J. Phys. Chem* **1998**, *102, 6685−6687.* (e) Ohara, P. C.; Heath, J. R.; Gelbart, W. M. *Angew. Chem., Int. Ed. Engl.* **1997**, *36*, 1080−1083.

(8) (a) Weiss, J. A.; Larsen, A. E.; Grier, D. G. *J. Chem. Phys.* **1998**, *109*, 8659−8666. (b) Wickman, H. H.; Korley, J. N. *Nature* **1998**, *393*, 445−447. (c) Pan, G.; Tse, A. S.; Kesavamoorthy, R.; Asher, S. A. *J. Am. Chem. Soc.* **1998**, *120*, 6518−6524. (d) Rakers, S.; Chi, L. F.; Fuchs, H. *Langmuir* **1997**, *13*, 7121−7124.

(9) (a) Taleb, A.; Petit, C.; Pileni, M. P. *J. Phys. Chem. B* **1998**, *102*, 2214−2220. (b) Taleb, A.; Russier, V.; Courty, A.; Pileni, M. P.; *Eur. Phys. J. B* **1999**, *59*, 13350−13358. (c) Pileni, M. P.; Taleb, A.; Petit, C. *J. Dispersion Sci. Technol.* **1998**, *22*, 696−702.

(10) (a) Holland, B. T.; Blanford, C. F.; Do, T.; Stein, A. *Chem. Mater.* **1999**, *11*, 795−805. (b) Holland, B. T.; Blanford, C. F.; Stein A. *Science* **1998**, *281*, 802−804. (c) Jiang, P.; Cizeron, J.; Bertone, J. F.; Colvin, V. L. *J. Am. Chem. Soc.* **1999**, *121*, 7957−7958. (d) Jiang, P.; Bertone, J. F.; Hwang, K. S.; Colvin, V. L. *Chem. Mater.* **1999**, *11*, 2132−2140.

(11) Brust, M.; Blass, P. M.; Bard, A. J. *Langmuir* **1997**, *13*, 5602−5607.

(12) Hu, K.: Brust, M.; Bard, A. J. *Chem. Mater.* **1998**, *10*, 1160−1165.

(13) Lvov, Y.; Ariga, K.; Onda, M.; Ichinose, I.; Kunitsake, T. *Langmuir* **1997**, *13*, 6195−6203.

(14) (a) Baum, T.; Bethell, D.; Brust, M.; Schiffrin, D. J. *Langmuir* **1999**, *15*, 866−871. (b) Fink, J.; Kiely, C. J.; Bethell, D.; Schiffrin, D. J. *Chem. Mater.* **1998**, *10*, 922−928.

(15) (a) Hostetler, M. J.; Green, S. J.; Stokes, J. J.; Murray, R. W. *J. Am. Chem. Soc.* **1996**, *118*, 4212−4213. (b) Terrill, R. H.; Postlethwaite, T. A.; Chen, C. H.; Poon, C. D.; Terzis, A.; Chen, A.; Hutchinson, J. E.; Clark, M. R.; Wignall, G.; Londono, J. D.; Superfine, R.; Flavo, M.; Johnson, C. S., Jr.; Samulski, E. T.; Murray, R. W. *J. Am. Chem. Soc.* **1995**, *117*, 12543−12548.

(16) Musick, M. D.; Peña, D. J.; Botsko, S. L.; McEvoy, T. M.; Richardson, J. N.; Natan, M. J. *Langmuir* **1999**, *15*, 844−852.

(17) Musick, M. D.; Keating, C. D.; Keefe, N. H.; Natan, M. J. *Chem. Mater.* **1997**, *9*, 1499−1502.

(18) Shipway, A. N.; Lahav, M.; Blonder, R.; Willner, I. *Chem. Mater.* **1999**, *11*, 13−15.

(19) Sarathy, K. V.; Thomas, P. J.; Kulkarni, G. U.; Rao, C. N. R. *J. Phys. Chem. B.* **1999**, *103*, 399−401.

(20) (a) Schrof, W.; Rozouvan, S.; Keuren, E. V.; Horn, D.; Schmitt, J.; Decher, G. *Adv. Mater.* **1998**, *3*, 338−341. (b) Anderson, M. L.; Morris, C. A.; Stroud, R. M.; Merzbacher, C. I.; Rolison, D. R. *Langmuir* **1999**, *15*, 674−681. (c) Antoine, R.; Pellarin, P.; Palpant, B.; Broyer, M. *J. Appl. Phys.* **1998**, *84*, 4532−4536. (d) De, G. *J. Sol-Gel Sci. Technol.* **1998**, *11*, 289−298. (e) Ye, S.; Vijh, A. K.; Wang, Z. Y.; Dao, L. H.; *Can. J. Chem.* **1997**, *75*, 1666−1669.

(21) (a) Mirkin, C. A.; Letsinger, R. L.; Mucic, R. C.; Storhoff, J. J. *Nature* **1996**, *382*, 607−609. (b) Storhoff, J. J.; Elghanian, R.; Mucic, R. C.; Mirkin, C. A.; Letsinger, R. L. *J. Am. Chem. Soc.* **1998**, *120*, 1959−1964.

(22) Marinakos, S. M.; Brousseau, L. C., III.; Jones, A.; Feldheim, D. L. *Chem. Mater.* **1998**, *120*, 1959−1964.

(23) (a) Hayat, M. A., Ed. *Colloial Gold: Principals, Methods, and Application*; Academic Press: New York, 1989; Vol. 1−3. (b) Turkevich, J.; Stevenson, P. C.; Hillier, J. *Discuss. Faraday Soc.* **1951**, *11*, 55−75. (c) Frens, G. *Nature Phys. Sci.* **1973**, *241*, 20−22.

(24) Doron, A.; Katz, E.; Willner, I. *Langmuir* **1995**, *11*, 1313−1317.

(25) (a) Garcia, M. E.; Baker, L. A.; Crooks, R. M. *Anal. Chem.* **1999**, *71*, 256−258. (b) Rubin, S.; Bar, G.; Taylor, T. N.; Cutts, R. W.; Zawodzinski, T. A., Jr. *J. Vac. Sci. Technol. A* **1996**, *14*, 1870−1877.

(26) (a) Chen, S.; Murray, R. W. *Langmuir* **1999**, *15*, 682−689. (b) Chen, S.; Murray, R. W. *J. Phys. Chem. B* **1998**, *102*, 9898−9907.

(27) Kreibig, U.; Vollmer, M. *Optical Properties of Metal Clusters*; Springer: Berlin, 1995.

(28) (a) Mulvaney, P. *Langmuir* **1996**, *12*, 788−800. (b) Foss, C. A., Jr.; Hornyak, G. L.; Stockert, J. A.; Martin, C. R. *J. Phys. Chem.* **1994**, *98*, 2963−2971. (c) Antoine, R.; Pellarin, M.; Palpant, B.; Broyer, M. *J. Appl. Phys.* **1998**, *84*, 4532−4536. (d) Klar, T.; Perner, M.; Grosse, S.; von Plessen, G.; Spirkl, W.; Feldman, J. *Phys. Rev. Lett.* **1998**, *80*, 4249−4252.

(29) (a) Grabar, K. C.; Freeman, R. G.; Hommer, M. B.; Natan, M. J. *Anal. Chem.* **1995**, *67*, 735−743. (b) Grabar, K. C.; Allison, K. J.; Baker, B. E.; Bright, R. M.; Brown, K. R.; Freeman, R. G.; Fox, A. P.; Keating, C. D.; Musick, M. D.; Natan, M. J. *Langmuir* **1996**, *12*, 2353−2361.

Scheme 1. General Multilayer Assembly Strategy

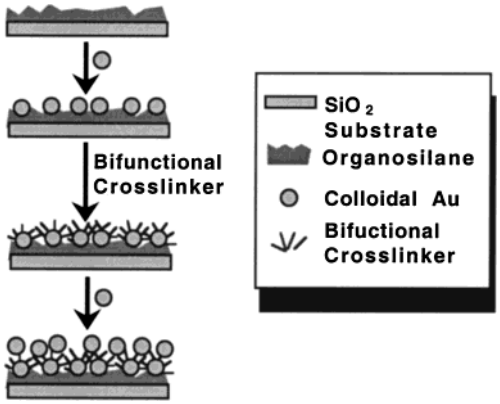

surface. (iv) Fabrication of patterned collections of nanoparticles has potentially important implications in nanoelectronic device fabrication and biosensing. In this regard, Natan and co-workers have previously characterized Au nanoparticle monolayer synthesis,[29,30] rate of assembly,[30] thermodynamics,[31] and morphology;[32] extension of assemblies into 3-D architectures may lead to new properties and broadened applications.

This paper describes a general methodology for assembling bulk metal-like films directly from solution in a stepwise fashion. It further illustrates possible applications in electrochemistry, biosensors, conductive coatings, surface patterning, and optical devices. Film formation, illustrated in Scheme 1, begins by repetitive immersions of a colloid-coated substrate into (i) a solution containing a bifunctional cross-linker and (ii) colloid metal sol (i.e., Au or Ag). In this manner, colloidal Au and Ag multilayer films as well as Au/Ag mixed metal films can be formed in a layer-by-layer fashion. Changes in topography, optical, and electrical properties have been monitored as a function of metal coverage and cross-linker identity.

Key results of these studies are as follows. (i) Film electrical conductivity and absorbance in the near-infrared (NIR) region is shown to depend on cross-linker length. Multilayer films composed of Au colloid and short bifunctional cross-linkers of ≤8 Å in length, at sufficient coverages, become very conductive. These are good examples of self-assembled electrodes with a high absorbance in the NIR region and an appearance similar to bulk Au. This contrasts with Au colloid multilayers fabricated with longer cross-linkers (≥8 Å) that have on average a 10^5 higher resistance and are transparent in the NIR region. (ii) Monitoring stepwise assembly using atomic force microscopy (AFM) and field emission scanning electron microscopy (FE-SEM) reveals a porous, aggregated nanostructure. The high film porosity (as well as biocompatibility) is confirmed by the fact that horseradish peroxidase-linked films remain enzymatically active, even after several layers of 11-nm diameter Au colloid are deposited. Two surface-sensitive techniques, surface plasmon resonance (SPR) and surface-enhanced Raman scattering (SERS), both sensitive to film roughness, have been used to probe the nanostructure. A thin Au film derivitized with Au colloid linked with 2-mercaptoethylamine shows a broadened SPR curve shifted more than 1° from the plasmon angle. Continued deposition of Au colloid layers results in greater perturbations; the shifts are found to be similar to those obtained for roughened Au films. SERS enhancement of adsorbed *trans*-1,2-(bis-4-pyridyl)ethylene (BPE) is observed after extended irradiation with monochromatic light or exposure to ozone, indicating that BPE adsorption is blocked by a cross-linker or that the enhancement occurs somewhere other than the outermost layer of colloids. Finally, it is shown that the porous multilayer structure can be replicated with good fidelity on patterned surfaces prepared by microcontact printing. The broad range of structures and properties illustrated by Au colloid multilayers suggests that solution-based, layer-by-layer assembly of metal films should be considered a complementary alternative to traditional methods of metal film preparation such as evaporation and plating.

Experimental Section

Materials. All H_2O used was from an 18 MΩ Barnstead Nanopure water filtration/purification system. Au and Ag colloids were synthesized in house, as described below. 3-Aminopropyltrimethoxysilane (APTMS), $HAuCl_4$, Na_3Citrate, 1,6-hexanedithiol, ethylenediaminetetraacetic acid dihydrate, disodium salt (EDTA), and *trans*-1,2-(bis-4-pyridiyl)ethylene (BPE) were purchased from Aldrich. The latter compound was recrystallized several times from a solution of CH_3OH and H_2O. The following materials were obtained from Sigma: horseradish peroxidase, 2-mercaptoethanol, 2-mercaptoethylamine (MEA), and Na_2SO_4. Concentrated HNO_3, HCl, NaOH, and H_2SO_4 were from J.T. Baker and 30% H_2O_2 was from VWR. Fisher Scientifc Co. glass microscope slides and spectrophotometry-grade CH_3OH were used. 3-Mercaptopropyltrimethoxysilane (MPTMS) and 3-mercaptopropylmethyldimethoxysilane (MPMDMS) were purchased from Gilest.

Benzidine and chloroform were obtained from Sigma Chemical Co. (St. Louis, MO). 4,4′-Diamino-*p*-terphenyl was obtained from Lancaster Synthesis Inc. (Windham, NH). Benzyltriethylammonium chloride and magnesium sulfate were obtained from Aldrich. Potassium hydroxide was obtained from EM Science (Gibbstown, NJ). Dichloromethane was obtained from Mallinckrodt (Phillipsburg, NJ).

Colloid Preparation. All glassware used for colloid preparation was thoroughly cleaned in aqua regia (3 parts HCl, 1 part HNO_3) and rinsed in deionized H_2O prior to use. A 12-nm Au colloid was prepared by citrate reduction of $HAuCl_4$ as described previously.[29,33] The resulting solution of colloidal particles had an absorption maximum at 518 nm. Sample analysis by transmission electron microscopy (TEM) indicated an average particle with major axis diameter of 10.7 nm ± 1.3 nm and a minor axis of 9.4 ± 1.1 nm from 221 particles sampled using NIH image software.

Polydisperse colloidal Ag was prepared from a literature protocol,[34] using EDTA reduction of aqueous $AgNO_3$. The Ag hydrosol produced had an intense plasmon absorption band at 402 nm.

Synthesis of Diisocyanophenylene Cross-linkers. Proton nuclear magnetic resonance spectra (^{1}H NMR) were obtained at 300 MHz on a Bruker AM-300 spectrometer. Diffuse reflectance Fourier transform infrared spectra (DRIFT)

(30) Grabar, K. C.; Smith, P. C.; Musick, M. D.; Davis, J. A.; Walter, D. G.; Jackson, M. A.; Guthrie, A. P.; Natan, M. J. *J. Am. Chem. Soc.* **1996**, *118*, 1148−1153.

(31) Keating, C. D.; Musick, M. D.; Keefe, M. H.; Natan, M. J. *J. Chem. Educ.* **1999**, *76*, 949−955.

(32) Grabar, K. C.; Brown, K. R.; Keating, C. D.; Stranick, S. J.; Tang, S. L.; Natan, M. J. *Anal. Chem.* **1997**, *69*, 471−477.

(33) Brown, K. R.; Natan, M. J. *Langmuir* **1998**, *14*, 726−728.

(34) (a) Bright, R. M.; Musick, M. D.; Natan, M. J. *Langmuir* **1998**, *14*, 5695−5701. (b) Lee, P. V.; Meisel, D. J. *J. Phys. Chem.* **1982**, *86*, 3391−3395.

were obtained on a Mattson Galaxy FT-IR. Electron ionization mass spectra (EIMS) were obtained on a Kratos MS25. Analytical thin-layer chromatography was performed using precoated silica gel (60 F_{254}) on aluminum plates obtained from Aldrich. Flash column chromatography was performed using Merck silica gel (grade 9385, 230−400 mesh, 60 Å) according to the procedures of Still et al.[35]

*1,4-Diisocyanobenzene (**1**).* Diisocyanide **1** was obtained from Aldrich and used without further purification.

*4,4′-Diisocyano-p-biphenylene (**2**).* Diisocyanides **2** and **3** were prepared using a modification of literature procedures.[36] A solution of 750 mg of benzidine dissolved in 450 mL of CH_2Cl_2 was placed in a 1000-ml, three-neck, round-bottomed flask equipped with a reflux condenser, magnetic stir bar, and a N_2 inlet. Into a 250-mL round-bottomed flask was placed 187.5 mL of a 50:50 (by weight) solution of KOH in H_2O. The solutions were degassed for 15 min and then combined, along with 5 mg of benzyltriethylammonium chloride dissolved in 2.5 mL of $CHCl_3$. The reaction mixture was refluxed for 4.5−5.5 h under constant stirring, an additional 2.5 mL of $CHCl_3$ added after 2 h. The mixture was then added to 450 mL of H_2O and the organic layer extracted in a separatory funnel and washed twice with 450 mL of H_2O and once with 450 mL of saturated NaCl solution. The CH_2Cl_2 was dried over $MgSO_4$, filtered, and evaporated in a rotary evaporator yielding a light brown crude product in 85% yield. TLC analysis, using 10% hexane in CH_2Cl_2, revealed that some monosubstituted 1-amino-4-isocyanobiphenylene was present. Both products were isolated using flash column chromatography with the 1:9 hexane/CH_2Cl_2 solution as the solvent. The more soluble light yellow, powdery product was removed from the column yielding 405.0 mg (54%) of **2**. R_f: 0.523. IR (KBr): ν(NC), 2128 cm^{-1}. ^1H NMR (300 MHz, $CDCl_3$): δ 7.49 (d, 4H), 7.63 (d, 4H). EIMS *m*/*z*: 204.2.

4,4′-Diisocyano-p-terphenylene (3). Diisocyananide **3** was prepared from the corresponding amine in a similar manner as described for **2**, with an 82% crude product yield and a 334.5-mg (44.6%) yield after chromatography. R_f: 0.786. IR (KBr): ν(NC), 2130 cm^{-1}. ^1H NMR (300 MHz, $CDCl_3$): δ 7.43 (d, 4H), 7.59 (d, 4H), 7.63 (s, 4H). EIMS *m*/*z*: 280.1.

Sample Preparation. Au colloid multilayer samples that were constructed for surface plasmon resonance and electrical and optical characterization were prepared on Fisher Premium microscope slides cut to approximately 0.9 × 2.5 cm rectangles. Substrates were cleaned with aqua regia (3:1 HCl:HNO_3), submerged in piranha wash (3:1 H_2SO_4:30% H_2O_2), and rinsed with H_2O. Substrates were modified by immersion into a 5% silane solution and multilayers were constructed by alternate immersions into colloidal Au and a bifunctional cross-linker solution [5 mM 2-mercaptoethanol or 2-mercaptoethylamine in H_2O, 1,6-hexanedithiol in CH_3CH_2OH, or **1**, **2**, **3** in CH_2Cl_2]. A vigorous rinse with H_2O is necessary between each step. Four Au bars (100 nm) at 0.5- and 1-cm spacing were evaporated across the width of the slide to provide contact for resistance measurements.

Ag monolayers were prepared as follows: clean glass substrates were silanized by reaction with 10% MPTMS in CH_3OH for 1−2 h, followed by extensive rinsing with CH_3OH and H_2O and exposure to colloidal Ag solution for 1−1.5 h. Multilayers were prepared from monolayers by treatment with 4 mM BME for 8−10 min, followed by extensive rinsing and exposure to colloidal Ag for 1−1.5 h. This process was repeated 0−9 times to produce surfaces with increasing amounts of Ag. Surfaces were rinsed in H_2O and then CH_3OH and dried in an 80 °C oven before storage in air.

Mixed-metal (Au/Ag) multilayers were prepared in a fashion similar to that of Ag multilayers, except that either Au or Ag colloid was used when Ag sol was used in the above description. All the initial monolayers were Au colloid on APTMS (10% in CH_3OH). Surfaces were dried as described for Ag multilayers.

Au Film Preparation. Thin (47−50-nm) Au films were prepared by thermal evaporation of Au shot (99.99%, Johnson Mathey) from a resistively heated Mo boat (Kurt J. Lesker) in a diffusion-pumped Edwards Auto 306 thin film fabrication system. Evaporation substrates were 1 × 1 × 0.02 in. pieces of polished SF11 glass (n = 1.78, Schott Glass Technologies) that had been exposed to a 10% (v/v) 3-mercaptopropyltrimethoxysilane/CH_3OH solution for 30 min to increase the adhesion of Au to the glass.[37] Au was deposited at a pressure of 1 × 10^{-6} mbar at 0.5 nm/s with constant sample rotation to ensure uniform deposition. Following evaporation, the films were annealed in a home-built glass tube oven at 300 °C for 5−10 min under a constant flow of Ar to decrease the surface roughness of the evaporated layer.

Instrumentation. Optical spectra were recorded on a HP-8452 diode array UV−vis or a Perkin-Elmer Lambda 9 scanning UV−vis/NIR. Au colloid coverage was calculated from atomic absorption spectrometry data from a Perkin-Elmer 1100B AAS. The sample area (6-mm diameter) was confined within a glass cell (O-ring sealed), digested in 50% aqua regia, and diluted to a known volume with H_2O. A Digital Instruments Nanoscope 3A operated in tapping mode at a 2-Hz scan rate and 512 lines per image was used to acquire topography scans and electric field measurements. Conductivity measurements were made in a typical two-point fashion using a home-built sample holder. A Keithley 6517A high-resistance electrometer or Fluke 77 multimeter was used to collect resistance data. UV light was generated with a Boekel Industries UV-Clean (model 135500).

SERS spectra were obtained by irradiating a sample with 107 mW of power from a Coherent Innova-70 Spectrum Laser (mixed Ar^+/Kr^+) at 647.1 nm. Scattered light was collected in a backscattering geometry and focused into a SPEX 1877 triple monochromator fitted with a 1200 g/mm grating in the spectrograph stage and two 600 g/mm gratings in the filter stage. The band-pass was 5 cm^{-1}. Detection was with a CCD detector cooled to 140 K. The spectrometer was calibrated using imidazole as a frequency standard. Each spectrum is the average of 10 acquisitions integrated for 10 s each.

Surface plasmon curves were measured using a home-built high-resolution scanning SPR instrument. Excitation of the surface plasmon was accomplished using the Kretschmann geometry where a 1-in. diameter hemispherical prism (SF11 glass, Esco Products) is index matched (Cargille Immersion Oil, n = 1.78) to a SF11 substrate onto which Au had been previously evaporated. This assembly was then affixed to a home-built flow cell (volume ≈ 100 mL) with the Au film exposed to solution. The SPR excitation source was a cylindrical 5-mW, 500:1 polarization extinction HeNe laser (632.8 nm, Melles Griot), which was further polarized by a 500:1 visible-optimized linear polarizer. An optical chopper (Stanford Research Systems) was used to modulate the optical signal at a frequency of 2 kHz that was then correlated with detection via a lock-in amplifier (Stanford Research Systems). The beam was focused by a 100-mm focal length (fl) plano-convex (PCX) lens and recollimated by a 25-mm fl PCX lens, thereby reducing the beam size to 0.4 ± 0.1 mm in diameter. A hemispherical lens was then used to focus the beam such that it was recollimated by the hemispherical prism-sample assembly. The reflected beam was then passed through an iris and focused onto a silicon photodiode detector (Thor Labs), the signal from which was then measured with the lock-in amplifier that was in-phase with the excitation source. Angular positioning of the sample was accomplished with a home-built $\theta-2\theta$ stage consisting of two high-resolution (0.001°) servo-drive rotation stages (Newport Corp.) that are mounted together such that their axes of rotation are collinear. The prism/sample/flow cell assembly was then mounted on the

(35) Still, W. C.; Kahn, M.; Mitra, A. *J. Org. Chem.* **1978**, *43*, 2923−2925.

(36) Henderson, J.; Feng, S.; Ferrence, G. M.; Bein, T.; Kubiak, C. P. *Inorg. Chim. Acta* **1996**, *242*, 115−125.

(37) Goss, C. A.; Charych, D. H.; Majda, M. *Anal. Chem.* **1991**, *63*, 85−88.

$\theta-2\theta$ stage such that the center of the Au/glass sample was at the axis of rotation. Stage rotation and data collection were controlled through a computer interface that was developed in-house with the LabVIEW programming language (v. 4.01, National Instruments). Typical SPR scan were run at either 0.1° or 0.01° resolution, a stage rotation rate of 0.5° s^{-1}, and a lock-in time constant of 0.3 s.

Results and Discussion

Sample Fabrication and Characterization. Multilayer films are generated in a stepwise fashion from Au or Ag hydrosols as depicted in Scheme 1. A monolayer of Au or Ag colloid on a silanized SiO_2 substrate (APTMS, MPTMS, MPMDMS) is briefly immersed in a dilute solution (5 mM, 10 min) of bifunctional cross-linker, scrupulously rinsed, and immersed in Au or Ag solutions (40−60 min), where additional particle binding occurs. Multilayer films result from repetitive exposure to the cross-linker and sol. There is no mechanism to ensure interlayer or intralayer registry between particles, nor is any expected. The inherent flexibility of the stepwise assembly process provides a platform for assembly of any combination of nanoparticles. In general, almost arbitrarily thick films of any size Ag or Au nanoparticle can be made using the protocol in Scheme 1, although derivatization times depend on particle concentration and size.

Photographs of multilayers assembled from Au and Ag metal nanoparticles are shown in Figure 1. Particle coverage increases from left to right in each. Films assembled from 11-nm diameter Au nanoparticles linked by MEA (top row) initially show a color change from pink to blue; after 15 exposures to MEA/Au colloid they have a final appearance similar to, in color and reflectivity, bulk Au, suggestive of bulk metal behavior. Comparable color shifts from yellow to green are observed with films composed of polydispersed MEA-linked Ag nanoparticles (bottom row), and at higher coverage, a bulk Ag appearance is observed. Composite films of alternating layers of colloidal Ag and Au undergo a similar color shift. Interestingly, a large portion of the visible spectrum is traversed by mixing just two types of particles. Such films might have applications as dichroic coatings. Figure 2 shows the optical absorbance spectra of such Ag/Au colloid multilayers both in H_2O (top) and in air (bottom). The spectra in H_2O are interesting in that they comprise the surface plasmon band of both Au colloid ($\lambda_{max} = 518$ nm) and Ag colloid ($\lambda_{max} = 408$ nm). Deposition of a layer of nanoparticle results in an increase at the respective λ_{max}. For example, the change in absorbance from 0.41 (top panel, curve b) to 0.60 (top panel, curve c) at $\lambda_{max} = 408$ nm indicates the addition of a layer of Ag particles. Previously, we demonstrated the increased λ_{max} due to the stepwise addition of Au nanoparticles obeyed Beer's law, even after >15 layers.[17] Notice only negligible change in absorbance occurs at $\lambda_{max} = 518$ nm. A similar observation can be made for the addition of an Au colloid layer (e.g., spectra d and e, top panel). Upon drying of the film, aggregation of the particles is indicated by a red shift in the λ_{max} and a broadening of the spectra. Information about the composition of the film is lost due to the combination of individual plasmon bands into collective plasmon oscillations (bottom panel).

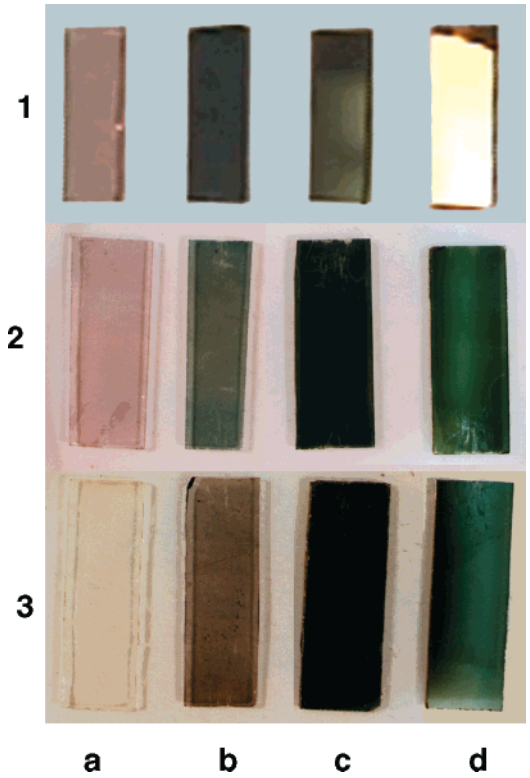

Figure 1. Photograph of Au, Au/Ag, and Ag nanoparticle multilayer samples. Au multilayers shown in row 1 are from left to right: Au colloid monolayer (a), after five treatments of colloid and four of 2-mercaptoethylamine (b), 12 colloidal Au layers (c), and 20 colloidal Au layers (d). Row 2: Au/Ag mixed-nanoparticle multilayers with exposures to either Au (11-nm diameter, 17 nM, 60 min) or Ag colloid and $HSCH_2CH_2OH$ (5 mM, 10 min). The film compositions are: (a) Au monolayer; (b) Au/Ag/Ag; (c) Au/Ag/Ag/Ag/Au; (d) Au/Ag/Ag/Ag/Au/Ag/Au. Row 3: $HSCH_2CH_2OH$/Ag colloid multilayers after 3 (a), 5 (b), 7 (c), and 9 (d) Ag treatments, respectively.

Likewise, optical spectra of Au and Ag (Supporting Information) colloidal multilayers display an increase in absorbance over the entire visible region (350−820 nm), corresponding to additional particle coverage with each cross-linker/colloid.

To develop functional nanostructured arrays with tailored properties, the ability to predetermine the nanoparticle coverage is essential. Previous efforts have focused on understanding nanoparticle monolayer formation from both kinetic[30] and thermodynamic perspectives.[31] To gain a more accurate view of the surface architecture, detailed analysis of film morphology was carried out using AFM and FE-SEM. These data indicate a porous, networked structure. AFM images (Figure 3) acquired on a 2-mercaptoethanol-linked colloidal Au multilayer as a function of the number of Au colloid layers reveal small segregated areas of agglomerated colloid that evolve into connected peaks of colloidal Au. By 11 Au layers, large areas of uninterrupted colloid form a porous interconnected network suggestive of conductive pathways. The AFM line scans (Supporting Information) depict an increase in film depth after each Au colloid treatment and the peaks and valleys associated with film formation. In contrast to AFM, which depicts a more closely packed film, the increased lateral resolution of FE-SEM reveals that discrete colloidal islands are present, even after expo-

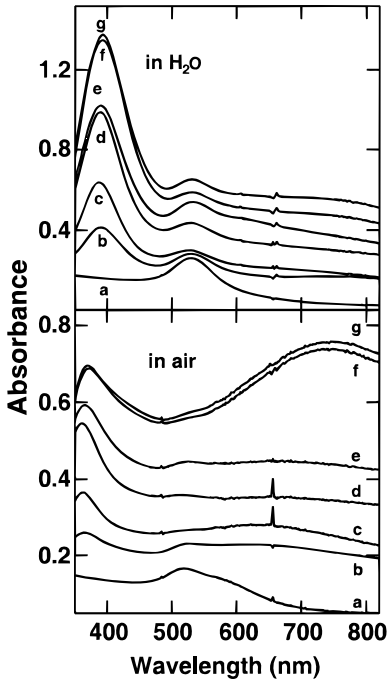

Figure 2. Optical absorbance spectra for Au/Ag mixed-nanoparticle multilayers with exposures to either Au (11-nm diameter, 17 nM, 60 min) or Ag colloid and $HSCH_2CH_2OH$ (5 mM, 10 min) wet (top) and dry (bottom). The film composition is: (a) Au monolayer; (b) Au/Ag; (c) Au/Ag/Ag; (d) Au/Ag/Ag/Ag/Au; (e) Au/Ag/Ag/Ag/Au/Ag; (f) Au/Ag/Ag/Ag/Au/Ag/Au.

sure of an Au colloid monolayer to a single additional layer of Au (Supporting Information). Interestingly, in a high-magnfication FE-SEM of an Au/Ag particle composite film (Supporting Information), the spherical monodisperse Au colloid is easily distinguished from the heterogeneous Ag nanoparticles.

Molecules with two or more functional groups capable of strong interactions with metallic Au can be used to cross-link colloidal Au particles. Table 1 lists cross-linkers used in this work. Functional groups used include thiol, amine, siloxane, alcohol, and isocyanide. Binding of the latter functional group to Au has been studied in detail by Angelici.[38] Kubiak and co-workers have previously described the binding of −NC-terminated phenylenes to Au clusters.[36] Likewise, thiol Au chemistry has been extensively probed with respect to self-assembled monolayer formation, and the synthesis of thiol-capped Au nanoparticles by the Schiffrin and Murray groups, among others, have extended characterization to Au nanoclusters.[14,15,39] Amine groups such as those on MEA or APTMS have previously been shown to electrostatically couple Au particles.[30] Indeed, low concentrations of each cross-linker added to a solution of colloidal Au cause flocculation.

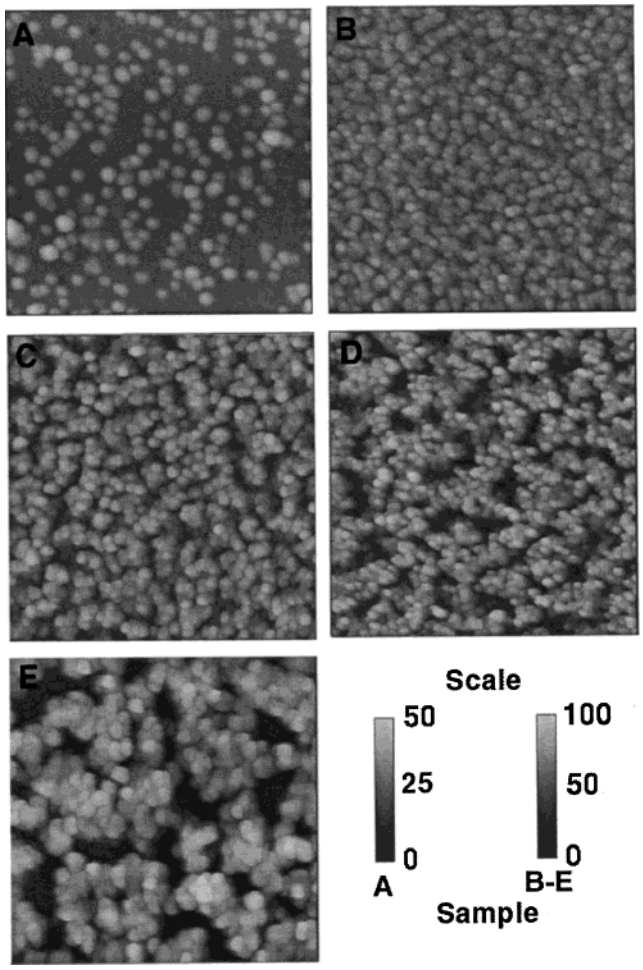

Figure 3. Tapping mode AFM (scan size $1 \times 1\ \mu$m) of $HSCH_2CH_2OH$-linked Au colloid multilayers: (A) monolayer; (B) 3 Au treatments; (C) 5 Au treatments; (D) 7 Au treatments; (E) 11 Au treatments.

The mechanism of colloid addition appears to be independent of cross-linker type, with all films displaying an increase in absorbance with each additional layer of colloid. Even multilayers constructed using protein cross-linkers of bovine serum albumin or horseradish peroxidase demonstrated a linear increase in absorbance and maintained enzymatic activity (Supporting Information), important results for the possibility of constructing biosensors or bioelectronics.[40,41] However, bulk optical properties are dramatically affected by the choice of cross-linker. Figure 4 shows UV−vis/NIR transmission spectra of Au colloid multilayer films prepared using three bifunctional cross-linkers [MEA (top), APTMS (middle), and 1,6-hexanedithiol (bottom)], as a function of the number of particle and cross-linker treatments. With MEA-linked films, a decrease in

(38) Ontko, A. C.; Angelici, R. J. *Langmuir* **1998**, *14*, 1684−1691.
(39) (a) Hostetler, M. J.; Wingate, J. E.; Zhong, C, -J.; Harrise, J. E.; Vachet, R. W.; Clark, M. R.; Londono, J. D.; Green, S. J.; Stokes, J. J.; Wignall, G. D.; Glish, G. L.; Porter, M. D.; Evans, N. D.; Murray, R. W. *Langmuir* **1998**, *14*, 17−30. (b) Templeton, A. C.; Hostetler, M. J.; Kraft, C. T.; Murray, R. W. *J. Am. Chem. Soc.* **1998**, *120*, 1906−1911. (c) Weisbecker, C. S.; Merritt, M. V.; Whitesides, G. M. *Langmuir* **1996**, *12*, 3763−3773. (d) Badia, A.; Singh, G. S.; Demers, L.; Cuccia, L.; Reven, L. *Langmuir* **1996**, *12*, 1262−1269. (e) Brust, M.; Fink, J.; Bethell, D.; Schriffin, D. J.; Kiely, C. *J. Chem. Soc., Chem. Commun.* **1995**, *98*, 1655−1656. (f) Brust, M.; Walker, M.; Bethell, D.; Schriffin, D. J.; Whyman, R. *J. Chem. Soc., Chem. Commun.* **1994**, *97*, 801−802.
(40) (a) Behnke, O.; Ammitzbell, T.; Jessen, H.; Klokker, M.; Nilusen, K.; Tranum-Jensen, *J. Eur. J. Cell. Biol.* **1986**, *41*, 326−338. (b) Khlebtstov, N. G.; Bogatyrev, V. A.; Dykman, L. A.; Mel'nikov, A. G. *Colloid. J.* **1995**, *57*, 412−423.
(41) (a) Stonehuerner, J. G.; Zhao, J.; O'Daly, J. P.; Crumbliss, A. L.; Henkens, R. W. *Biosens. Bioelectron.* **1992**, *7*, 421−428. (b) Zhao, J.; Henkens, R. W.; Stonehuerner, J. G.; O'Daly, J. P.; Crumbliss, A. L. *J. Electroanal. Chem.* **1992**, *327*, 109−119. (c) Crumbliss, A. L.; Perine, S. C.; Stonehuerner, J. G.; Tubergen, K. R.; Zhao, J.; Henkens, R. W.; O'Daly, J. P. *Biotechnol. Bioeng.* **1992**, *40*, 483−490. (d) Zhao, J.; O'Daly, J. P.; Henkens, R. W.; Stonehuerner, J.; Crumbliss, A. L. *Biosens. Bioelectron.* **1996**, *11*, 493−502. (e) Brown, K. B. Ph.D. Thesis, Pennsylvania State University, University Park, PA, 1997.

Table 1. Cross-linkers Used To Form Multilayers

Crosslinker	Length (Å)
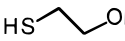	5.6[a]
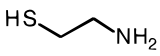	8.0[a]
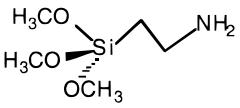	9.1[a]
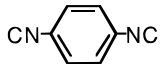	9.5[a]
	11.3[a]
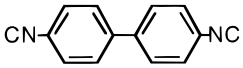	12.4[a]
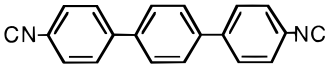	16.9[a]
Bovine Serum Albumin	143[b]
Horse Radish Peroxidase	140 x 40 x 40[c]

[a] Energy minimized length. [b] From the structure described in Gajhede, M.; Schuller, D. J.; Henriksen, A.; Smith, A. T.; Poulos, T. L. *Nat. Struct. Biol.* **1997**, *4*, 1032−1035. [c] From the crystal structure described in Bendedouch, D.; Chen, S. H. *J. Phys. Chem.* **1983**, *87*; 1473−1477.

transmission is seen from ≥90% between 800 and 2500 nm to ≤15% with nine layers of particles. The high degree of reflectivity over a broad wavelength range is typical of metallic behavior.[42] Colloidal Au multilayers comprised of nine or more layers appear, to the eye, indistinguishable from evaporated Au films (Figure 1) and have a UV−vis/NIR spectra comparable to evaporated metal films[42] and films generated by reduction of Au^{3+} onto an Au colloid monolayer.[33] This suggests similarities between films of closely packed Au nanoparticles and bulk Au films. Moreover, linked colloid multilayer films, Au-plated films, and evaporated Au films turn from blue to a metallic gold luster as the Au coverage is increased. We previously reported that as in evaporated metal films, 2-mercaptoethanol-linked multilayer films also undergo the same large decrease in %*T*.[17]

The transmission in the NIR region is nearly wavelength independent for 2-mercaptoethanol- and MEA-linked Au colloid multilayers.[17] In contrast, films generated from longer cross-linking molecules (APTMS, 1,6-hexanedithiol, and diisocyanides) exhibit markedly different optical properties. With APTMS-linked Au colloid multilayers, the transmittance in the visible region decreases linearly as a function of colloid coverage, as with MEA. However, the NIR region remains relatively transparent, and wavelength dependent. Similar results are obtained with 1, 6-hexanedithiol-linked films. A comparison of the optical spectra with molecular structures in Table 1 demonstrates that films assembled from shorter cross-linkers resemble bulk Au, suggesting that a collective particle mode contributes to the NIR absorption behavior. Interestingly, a difference of only ≈1.5 Å in molecular length results in significant differences in optical properties. A series of aryl diisocyanides were synthesized for a controlled study of cross-linker length (Table 1) versus optical properties (Figure 5). Despite a 7-Å difference in cross-linker length between **1**, **2**, and **3**, the optical properties in the visible region 400−800 nm are nearly indistinguishable. After greater than 20 cross-linker/Au colloid treatments (11-nm diameter), films are less than 5% transmissive at 600 nm and to the eye appear dark blue. Films prepared from **1** display strong wavelength dependence in the near-IR region, similar to APTMS-linked films of comparable coverage. It is interesting to note that the predicted difference in length for these two molecules is ≤1 Å. Films prepared using **2** and **3** also have a wavelength-dependent transmission, but it is less pronounced; moreover, the films are more transmissive. Thus, at 1500 nm, with 20+ layers, films made using **1** are 40% transmissive, while those of **2** and **3** are 60% transmissive.

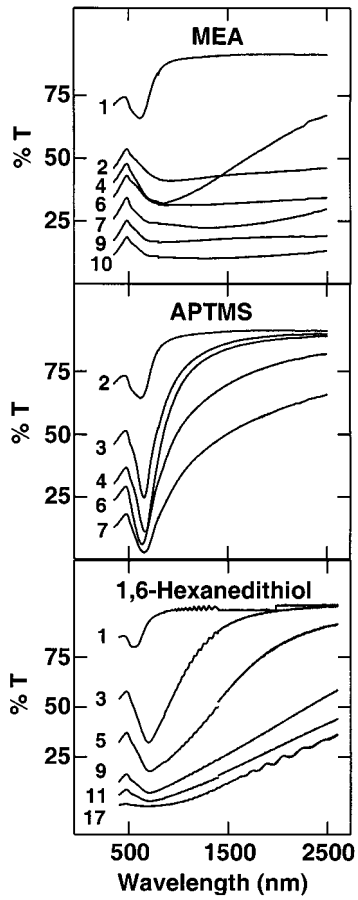

Figure 4. UV−vis/near-IR transmission spectra of colloidal Au multilayers on MPTMS-coated as a function of the number of layers of 12-nm diameter colloidal Au particles (monolayer = 1) for the cross-linkers 2-mercaptoethylamine (top), APTMS (middle), and 1,6-hexanedithiol (bottom).

The data in Figures 5 and 6 suggest that the optical properties of colloidal metal nanoparticle films are

(42) (a) Aspnes, B. *Thin Solid Films* **1982**, *89*, 249−263. (b) Yagil, Y.; Deutscher, G. *Thin Solid Films* **1987**, *152*, 467−471. (c) Sarychev, A. K.; Bergman, D. J.; Yagil, Y. *Phys. Rev. B* **1995**, *51*, 5366−5385. (d) Heavens, O. S. *Optical Properties of Thin Solid Films*; Dover Pulications: New York, 1991.

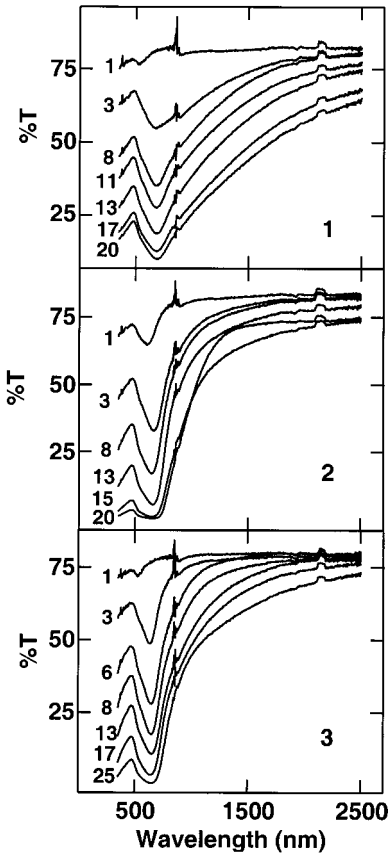

Figure 5. UV−vis/near-IR transmission spectra of 12-nm diameter Au colloid multilayers cross-linked with 1,4-diisocyanobenzene (**1**), 4,4′-diisocyano-*p*-biphenylene (**2**), and 4,4′-diisocyano-*p*-terphenylene (**3**).

described by four distinct ranges determined by the interparticle spacing of the Au nanoparticles. (i) Colloid films fabricated from cross-linkers with a molecular length (ML) ≤8 Å display properties much like their bulk metal counterparts: a broad surface plasmon band, wavelength independence from 800 to 2500 nm, and a linear decrease in transmission from 350 to 2500 nm with each colloid treatment. (ii) For films where cross-linker ML is 8 < ML < 12 Å, intermediate behavior is observed; a decrease in transmission is observed with the addition of Au colloid from 300 to 800 nm, the particle plasmon band is visible even at high coverage, and there is a moderate wavelength dependence observed between 800 and 2500 nm. Contrary to this behavior, the transmission spectra of films generated from 1,6-hexanedithiol and Au colloid have properties that resemble films assembled from shorter cross-linkers [i.e., APTMS or **1**]. This suggests the possibility that both ends of the dithiol may be bound to the same particle, thereby allowing two colloids to approach each other closer than predicted. (iii) For films with cross-linker ML > 12 Å the visible region is identical, between 700 and 1000 nm a strong wavelength dependence is observed, and from 1000 to 2500 nm the films are transparent with no observed wavelength dependence, even with as many as 25 treatments of cross-linker and colloid. These regions are not unlike the regions described by scaling theory and effective medium approximations (Maxwell−Garnet, MG) used to model the optical and electrical behavior of discontinuous metal

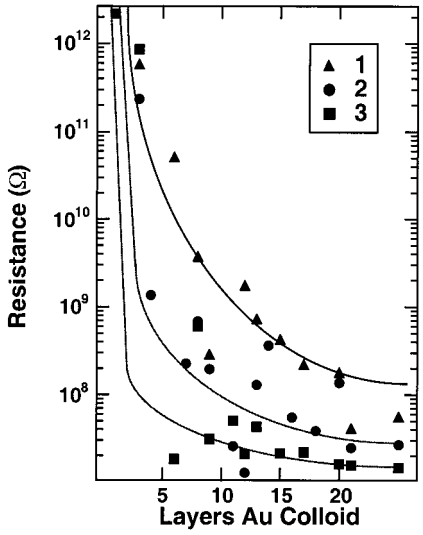

Figure 6. dc resistance immobilized colloidal Au (11-nm diameter) multilayers linked by **1** (■), **2** (●), and **3** (▲).

films, cermets, and polymer composites.[43] Both models describe the dielectric properties of a conductor in a dielectric matrix by calculating a composite dielectric based on the volume fraction of conductor. Finally, (iv) when the cross-linker dimensions are of the same order of magnitude as the particles, i.e., multiple nanometers (as in BSA and HRP), there is no interaction between particles, and the multilayers remain essentially transparent in the near-IR region. The ability to precisely tune optical properties for an *arbitrary thickness* differentiates Au colloid multilayers from evaporated films where, for a given thickness, the optical properties are relatively fixed.

Both the dimension of the spacer and the way multilayers are prepared could conceivably impact the film's volume fraction of metal, in the case of Au colloidal multilayers V_{Au}. Importantly, the precise volume fraction depends on the method of calculation. Note, however, that V_{Au} remains essentially unchanged with each colloid treatment (for each method of calculation). Determining V_{Au} from only AFM data, film volume, and maximum and average film heights results in V_{Au} values of 0.5 ± 0.02 and 0.1 ± 0.03, respectively. A $V_{Au} = 0.5$ is obtained from the film volume calculated by integrating the area under the peaks at the maximum film depth in an AFM. From a random sequential absorption model, the maximum packing for hard spheres results in a volume fraction of approximately 0.5.[44] However, this is the maximum possible volume fraction since the AFM is incapable of delineating volume under a feature. For example, a stack of spheres is viewed as a domed cylinder despite a significant contribution to the total film volume from the void volume. Other attributes of the multilayer system should cause substantial deviation from this model as well. For example, initial colloid placement is not random. Colloids have a negative charge and deposit with an average interparticle spacing greater than that

(43) (a) Maxwell−Garnet, J. C. *Philos. Trans. R. Soc. London, Ser. A* **1904**, *203*, 385. (b) Berthier, S.; Peiro, J. *J. Phys.: Condens. Matter* **1998**, *10*, 3679−3694. (c) Yagil, Y. Gadenne, P.; Julien, C.; Deutscher, G. *Physica A* **1994**, *207*, 360−364.

(44) Torquato, S. *Phys. Rev. Lett.* **1995**, *74*, 2156−2159.

predicted by random sequential absorption. Likewise, most cross-linkers are selective only for metal. Therefore, the deposition of additional layers is confined to regions previously occupied by colloids. Thus, a decrease in the predicted V_{Au} is expected. Similarly, a $V_{Au} = 0.1$ is below the volume fraction predicted for a 2-D or 3-D array of conductors (equal to 0.5 and 0.3, respectively),[45] yet these films can be remarkably conductive (see below). When particle size and coverage are determined by TEM and atomic absorption spectrometry, intermediate volume fractions are found. Total Au volume is found by AA and from the volume occupied by each nanoparticle the number of particles per unit area is determined. Considering the total volume occupied by Au and the total volume from the size and maximum height of the AFM scan area, a $V_{Au} = 0.21 \pm 0.04$ is found. This is in good agreement with the volume fraction determined from the diameter of the particle and the coverage of $V_{Au} = 0.23 \pm 0.04$. This method assumes that film height is increased only by one colloid diameter per treatment and uses the coverage information to determine the amount of colloid deposited. These are considered to be the best measures of volume fraction. Due to the mountain-like nature of the films, V_{Au} is extremely dependent upon the depth with the possibility of a higher V_{Au} in the lower layers. The important point from these calculations is that, irrespective of the method used, these are not significant changes in volume fraction during growth.

Electrical properties of discontinuous metal films and mixed metal particle composites have been demonstrated to depend on the volume fraction of metal.[45,46] Scaling law predicts a dimensionality-dependent critical point, p_c, where at the metal−insulator transition $p_c = V_{Au}$. For a 2-D case, p_c equals 0.5 and is between 0.25 and 0.31 for a 3-D system.[45] These values have been explored experimentally numerous times in simple systems, such as discontinuous metal films,[46] coevaporated materials,[47] or physical mixtures of carbon and Teflon particles.[48] For Au colloid films generated from short cross-linkers, 2-mercaptoethylamine and 2-mercaptoethanol (Supporting Information), the sharp decrease in resistance observed for each cross-linker after 5−6 exposures to Au colloid can be attributed to a change in dimensionality (from 2-D to 3-D). For 2-mercaptoethanol-linked films, the most conductive final resistance (70 Ω) is reached after 10 layers of Au colloid. This corresponds to a resistivity equal to 2×10^{-4} Ω/cm, approximately 200 times lower than that of bulk Au. As described above, V_{Au} is constant and approximately 0.23 for all Au coverages (11-nm diameter), in reasonable agreement with the predicted V_{Au} of 0.25 for a 3-D system. Gadenne and co-workers noted similar behavior in Au/Al_2O_3 composite films, where a critical film height

Scheme 2. Electrostatic Force Microscopy Detection Strategy

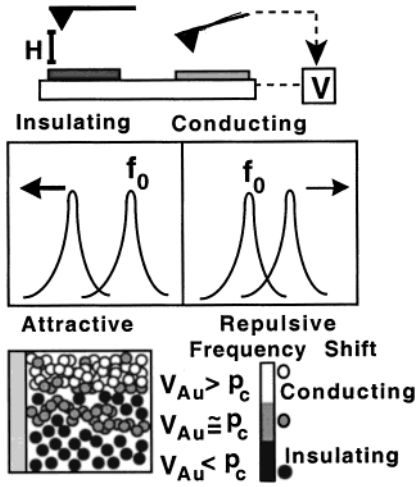

indicated the onset of conductivity.[49] However, germane to conductivity measurements is a second explanation in which a change in local volume fraction due to heterogeneity in the conductor dispersion results in planes of varying volume fraction. Such an explanation was offered to explain anomalous optical absorbance of Au particle/SiO_2 dispersions[47b] and may apply to the morphology of Au colloid multilayers. In comparison to conductive films cross-linked by MEA or 2-mercaptoethanol, films of 1,6-hexanedithiol, a longer cross-linker, reach a minimum resistance of 1 MΩ. Similar behavior is observed for multilayers linked by the diisocyanophenylene's **1**, **2**, and **3**, displayed in Figure 6. Once again, a decrease in resistance occurs after the addition of 4−5 layers of colloid, but the final minimum resistances for cross-linkers **1**, **2**, and **3** are 5, 18, and 35 MΩ, respectively−10^5 larger than that for shorter cross-linkers. Here, a correlation is observed between the minimum resistance and the length of the molecule; in this sense, dc resistance is comparable to the optical properties. Similar systems consisting of thiol-coated Au nanoparticles (<5-nm diameter) have been examined by the Murray group,[15] but no systematic examination of binding chemistry or particle size vs conductivity was reported.

Another way to consider the conductivity properties of these multilayers is through a scaling law, which describes conductivity as the fusion of isolated clusters into larger and larger clusters until a conductive pathway is formed across the surface.[45] At the metal−insulator transition a finite number of pathways are present. Few techniques are capable of discerning these conductive regions from the insulating ones. Notable exceptions are the electron[50] and scanning probe microscopies.[51] We used electric force microscopy (EFM) to image the charged region of a multilayer surface held at a positive voltage. The contrast mechanism for EFM is pictured in Scheme 2, in which the substrate is held

(45) Clerc, J. P.; Giraud, G.; Laugier, J. M.; Luck, J. M. *Adv. Phys.* **1990**, *39*, 191−309.

(46) (a) Connort, M. T.; Roy, S.; Ezquerra, T. A.; Calleja, F. *J. Phys. Rev. B* **1998**, *57*, 2286−2294. (b) McLachlan, D. S.; Heiss, W. D.; Chiteme, C.; Wu, *J. Phys. Rev. B* **1998**, *58*, 13558−135564. (c) Abeles, B.; Sheng, P.; Coutts, M. D.; Arie, Y. *Adv. Phys.* **1975**, *24*, 408−459. (d) Smilauer, P. *Contemp. Phys.* **1991**, *32*, 89−102.

(47) (a) Cohen, R. W.; Cody, G. D.; Coutts, M. D.; Abeles, B. *Phys. Rev. B* **1973**, *8*, 3689−3701. (b) Doyle, W. T. *J. Appl. Phys.* **1999**, *85*, 2323−2328.

(48) Aong, Y.; Noh, T. W.; Lee, S.-I.; Gaines, J. R. *Phys. Rev. B* **1986**, *33*, 904−908.

(49) Gadenne M.; Gadenne, P. *Thin Solid Films* **1992**, *221*, 183−190.

(50) Barkay, Z.; Dwir, B.; Deutscher, G.; *Appl. Phys. Lett.* **1989**, *55*, 2787−2789.

(51) (a) Houze, F.; Meyer, R.; Schneegans, O.; Boyer, L. *Appl. Phys. Lett.* **1996**, *13*, 1975−1977. (b) Viswanathan, R.; Heaney, M. B. *Phys. Rev. Lett.* **1995**, *75*, 4433−4436. (c) Chorniy, V. Z.; Adkins, C. *J. Phys. Rev. B* **1996**, *53*, 9606−9609.

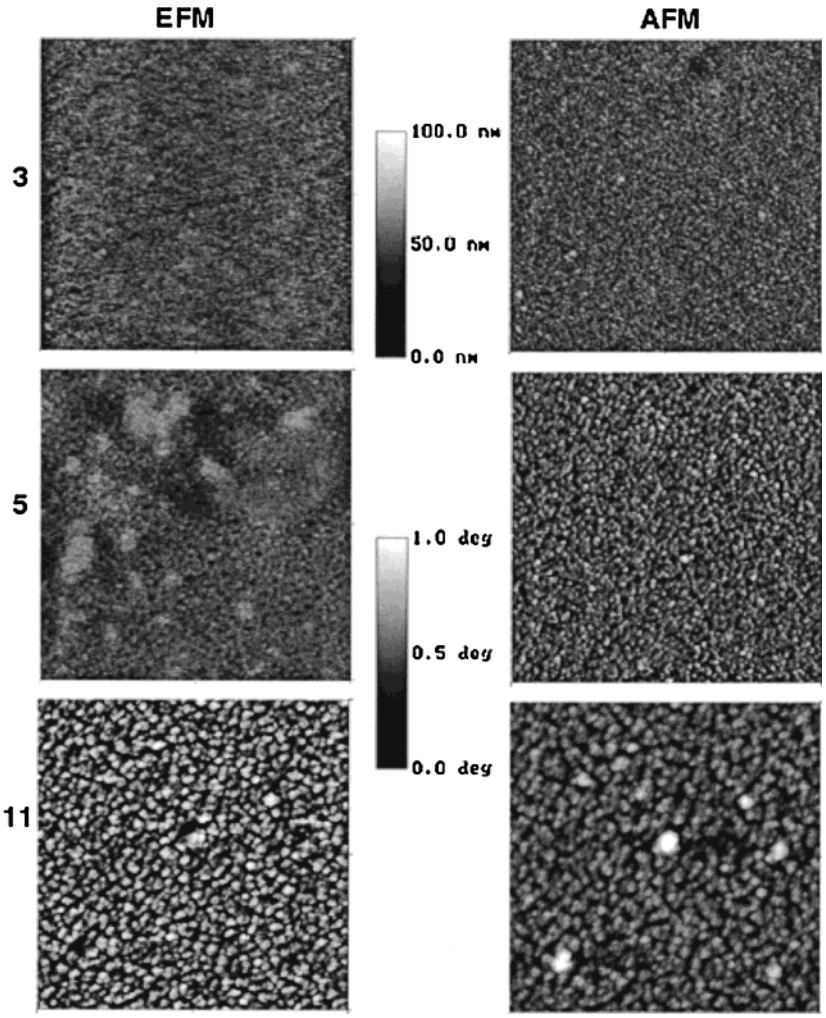

Figure 7. Electrostatic force microscopy images (left) and AFM images (right) of 12-nm diameter Au MEA-linked colloid multilayers (number of layers indicated on graph). EFM images (scan size 5 × 5 μm) collected at 2 V at a 1-Hz scan rate with a lift height of 25 nm.

at a positive potential and the tip is a fixed height above the surface. The phase modulation of an oscillating conductive probe is measured. The magnitude of the shift in frequency from the fundamental frequency, f_0, is a function of the potential difference between the tip and the surface. The direction of the shift is descriptive of the interaction force. A positive frequency shift indicates a repulsive force between the tip and the surface, and an attractive force is indicated by a negative shift. Figure 7 shows simultaneously acquired EFM (left) and topographic AFM (right) images of Au colloid multilayer films as a function of the number of colloid exposures. At 3 treatments the EFM resembles the corresponding AFM image. The phase is weakly dependent on film morphology. Strikingly, after 5 Au layers, approximately where the metal−insulator transition is located from the resistance data, island structures are apparent in the EFM image. If the potential is increased, an enhancement in contrast is observed (Supporting Information). Similar features were observed in high-density polyethylene and carbon black (80-nm mean diameter) composites by Viswanathan and Heaney[51b] using an EFM technique. In their work a critical volume fraction was found to be 0.19, comparable to 0.21−0.23 for Au colloid multilayers. However, the dimensionality of the carbon black composite was determined to be 2.6. Likewise, preliminary evidence on colloidal Au multilayers from electrochemical data and AFM suggests a fractal dimension between 2 and 3 and consequently comparisons to critical values of the scaling law are tentative. Few examples of this type of behavior appear in the literature; a detailed fractal analysis is in progress.[52] By the time 11 layers of Au colloid have been deposited, the contrast in the EFM images are lost because the entire film is conductive. The ability to monitor the development of conductivity in these films at the nanoscopic level complements nicely the bulk optical and electrical measurements described earlier. These data further suggest that near field scanning optical microscopy investigation of samples on the verge of becoming conductive (in the bulk) may show dramatically different optical properties on the nanometer scale.

Applications of Au Colloid Multilayers. The ability to generate conductive films from inexpensive solutions of metal nanoparticles offers applications in device fabrication, particularly on rough or sensitive substrates. Previously, we examined the electrochemical properties of Au colloid multilayers, finding that highly

(52) Richardson, J. N.; McEvoy, T. M.; Peña, D. J.; Musick, M. D.; Natan, M. J., in preparation.

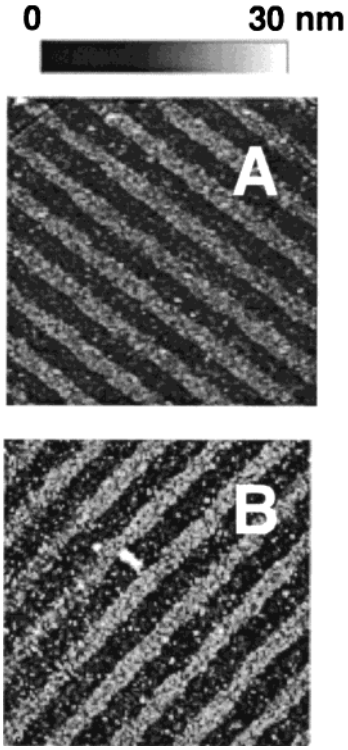

Figure 8. AFM (scan size 10 × 10 μm) of Au microcontact printed surfaces, where the initial stamp was inked with $HOOC(CH_2)_{15}SH$ to create a pattern "inert" to colloidal Au. This surface was then exposed to an aqueous 1.0 mM solution of MEA to render the interstices reactive toward colloidal Au. This treatment was then followed by (A) one exposure of the substrate to a 17 nM solution of 12-nm diameter colloidal Au and (B) two sequential MEA/Au exposures.

conductive, biocompatible, and facile electrodes could be constructed on a variety of substrate materials.[16] Figure 8 shows AFM images of a patterned multilayer surface made by microcontact printing.[53] In this technique a polymeric negative of an object is constructed by polymerization of a poly(dimethylsiloxane) (PDMS) solution containing the master (a grating with a 3-μm period). After hardening, the object is removed and an imprint remains in the polymer. In Figure 8, the PDMS negative was "inked" with $HOOC(CH_2)_{15}SH$, a molecule with a relatively low affinity for colloidal Au. The surface was then treated with MEA to fill in the interstices and subsequently exposed to a solution of 11-nm diameter Au colloid (Figure 8A). The pattern was developed further with two additional exposures to MEA and Au colloid (Figure 8B). A replica of the original grating surface is apparent in each image. Some nonspecific colloid binding is observed between the lines; clearly, there is some binding of Au to carboxylate. Nonetheless, the images show that multilayers of 12-nm diameter colloidal metal particles can be formed on patterned surfaces.[7e]

Au colloid multilayers can also be used for SPR and SERS, surface spectroscopies traditionally carried out with continuous Au films. SPR is a probe of film dielectric properties, film thickness, and morphology. In SPR, a prism-coupled attenuated total reflection technique, the angle-dependent reflectivity of an incident laser beam is measured. At a critical angle (the plasmon angle), all the incident energy is converted into a charge density oscillation and dissipated as heat. Thus, a

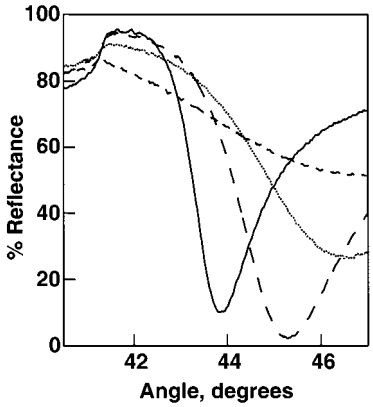

Figure 9. Surface plasmon resonance curves of a 39-nm thick evaporated Au film (—) and identical films treated with one (— — —), two (···), and three (- - -) successive exposures to 1.0 mM MEA in CH_3CH_2OH and 17 nM 12-nm diameter colloidal Au.

minimum in reflectivity is recorded. Several detailed treatments of SPR theory have been published.[54] Note that the evanescent wave penetrates a distance approximately $\lambda/2$ above the metal film and decays exponentially to zero.[54] It is this behavior, modeled by the Fresnel equations, that allows the film thickness and dielectric constant to be determined for several discrete layers of dielectrics.[55] Figure 9 shows SPR scans of a bare Au film (39-nm thick) and after 1, 2, and 3 exposures to MEA/11-nm diameter colloidal Au. After one treatment of Au colloid, a decrease in percent reflectivity, a 1.4° shift in plasmon minimum, and an overall broadening of the curve are observed. A 5-nm thick film of organic or protein molecules would result in only a 0.2° shift in reflectivity with no band broadening or change in percent reflectivity. The Fresnel equations assume a homogeneous dielectric constant of the absorbed layers and do not include scattering or absorption processes by metal nanoparticles. Furthermore, individual metal nanoparticles can support plasmon propagation at critical wavelengths.[27,28,56] These effects are believed to contribute significantly to the perturbations in the SPR curves, particularly the possibility that individual Au colloids may act as nanoscale roughness features. Previously, similar results were obtained for Ag films with 50-, 100-, and 200-nm underlayers of CaF_2:[57] the surface roughness of CaF_2 increases with thickness. Related experiments were conducted with LiF and an Au overlayer.[57] Also note that enhanced scattering and light emission have both

(53) (a) Kumar, A.; Whitesides, G. M. *Appl. Phys. Lett.* **1993**, *14*, 2002−2004. (b) Wilbur, J. L.; Kim, E.; Xi, Y.; Whitesides, G. M. *Adv. Mater.* **1995**, *7*, 649−652. (c) Xia, Y.; Whitesides, G. M. *Langmuir* **1997**, *13*, 2059−2067.

(54) (a) Pockrand, I. *Surf. Sci.* **1978**, *72*, 577−588. (b) Economou, E. N. *Phys. Rev.* **1969**, *182*, 539−554. (c) Raether, H. *Surface Plasmons on Smooth and Rough Surfaces and on Gratings*; Springer Tracts in Modern Physics 111; Springer-Verlag: Berlin, 1988.

(55) (a) Peterlinz, P.; Georgiadis, R. *Opt. Commun.* **1996**, *130*, 260−266. (b) John, M. S.; Radhakrishnan, P.; Nampoori, V. P. N.; Vallabhan, C. P. G. *Meas. Sci. Technol.* **1999**, *10*, 17−20. (c) Phelps, J. M.; Taylor, D. M. *J. Phys. D: Appl. Phys.* **1996**, *29*, 1080−1087.

(56) (a) Lyon, L. A.; Peña, D. J.; Natan, M. J. *J. Phys. Chem. B.* **1999**, *103*, 5826−5831. (b) Lyon, L. A.; Musick, M. D.; Natan, M. J. *Anal. Chem.* **1998**, *70*, 5177−5183.

(57) (a) Ferguson, A. J. L.; Dawson, P.; Walmsley, D. G. *J. Mod. Opt.* **1993**, *40*, 1725−1730. (b) Hoffmann, A.; Lenkefi, Z.; Szentirmay, Z. *J. Phys.: Condens. Matter.* **1998**, *10*, 5503−5513.

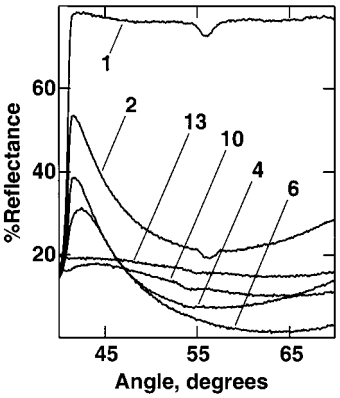

Figure 10. Surface plasmon resonance curves taken at 632.8-nm excitation for a series of multilayers on APTMS-coated glass prepared via successive immersion in aqueous solutions of 12-nm diameter colloidal Au and 2-mercaptoethylamine. The curve labels indicate the number of colloidal Au treatments, where "1" is a monolayer, "2" is a bilayer, and so forth.

been noted for roughened films of Au and Ag.[54c,58]

Multilayers assembled directly onto functionalized glass substrates (i.e., with no Au film) display a broad reflectivity band as a function of angle with 632.8-nm irradiation, even after 13 treatments of colloid (Figure 10). Interestingly, these films are highly conductive and appear like bulk Au to the eye. However, when examined by SPR, a minimum in the reflectance curve is apparent with the first two treatments, but disappears at succesive treatments. This contrasts with bulk Au, which at a critical thickness, displays a sharp minimum in percent reflectance. A minimum percent reflectance is observed after 6 treatments. Increasing Au colloid treatment results in a flat featureless spectrum with ≈20% reflectance. Very similar curves were obtained for 526.8-nm excitation (Supporting Information). Comparable behavior has been noted for reflectivity measurements for 50-nm thick granular Ag.[59] In this work, the primary mechanism was attributed to volume scattering from the bulk of the film due to a continuum of roughness sites that distribute the impinging radiation,[54c] and simultaneous measurement of the transmitted light confirmed the existence of radiative surface plasmons in a broad region around the plasmon angle. Due to the roughness of Au colloid multilayer films as discussed above, a scattering mechanism is suspected in the broad SPR curves for multilayers. Note at visible excitation the plasmon propagation length is >5 μm; for a film composed of 11-nm diameter particles such large areas of interrupted particle contact would be unusual.

The roughness associated with the colloid multilayer film might be well-suited to surface-enhanced Raman scattering. SERS has been under extensive scrutiny since its discovery.[60] Theory predicts as much as 10^{12} enhancement in Raman scattered photons for molecular vibrations perpendicular to an ideal SERS enhancing substrate.[61] Typical substrates include aggregated metal nanoparticle clusters,[62] electrochemically roughened Ag films,[63] and colloid monolayers.[64] The film nanostructure has a profound effect on the observed enhancement.

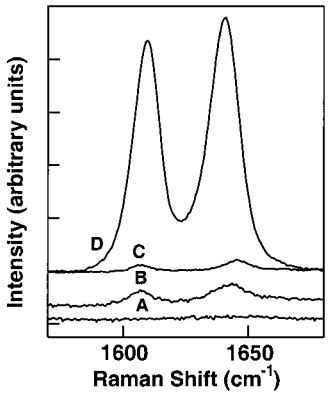

Figure 11. Effect of UV exposure upon SERS spectra for BPE adsorbed to a multilayer surface comprising 9 layers of Ag particles cross-linked by 2-mercaptoethanol. Spectra shown are for 10 mM BPE (A), the as-prepared multilayer surface in 10 mM BPE (B), and for the same surface in 10 mM BPE following exposure to UV radiation for 2 min (C) and 5 min (D). Conditions: 107 mW of 647.1-nm excitation at the sample, 5-cm^{-1} band-pass, 10-s integration × 10 accumulations.

In this regard, Natan and co-workers have reported combinatorially designed SERS substrates fabricated by electroless deposition of Ag onto Au colloid arrays.[65] Figure 11 shows a SERS spectra for BPE absorbed on an Ag nanoparticle 2-mercaptoethanol-linked multilayer. The spectra for 10 mM BPE solution with 647.1-nm excitation is featureless (A), and for an as-prepared multilayer, two weak peaks at 1605 and 1645 cm^{-1} are visible (B). Interestingly, after exposure to UV radiation for 5 min prior to BPE exposure, there is a substantial increase in the observed SERS spectra (D), suggesting that organic material blocked BPE adsorption. Possible explanations are that 2-mercaptoethanol rearranges to coat the topmost portion of the Ag multilayer and could shield BPE absorption onto the surface or that the active sites responsible for the SERS signal are not solely due to BPE confined to the topmost layer of colloid. The electric field enhancement may occur between two or more colloids. Indeed, Natan and co-workers have reported an SERS enhancement from metal nanoparticle sandwiches using cytochrome *c* as a probe molecule.[66] A comparable increase in intensity was found for mixed Au and Ag nanoparticle multilayers after extended irradiation with 647.1-nm light (Supporting Information). Presumably, enhancement is due to the heat- or ozone-induced removal of excess 2-mercaptoethanol and/or rearrangement of the colloid multilayer film.

(58) Vinogradov, E. A.; Leskova, T. A.; Ryabov, A. P. *Opt. Spectrosc.* **1994**, *76*, 311−322.
(59) Horstmann, C. *Opt. Commun.* **1977**, *6*, 176.
(60) Jeanmarie, D. L.; Van Duyne, R. P. *J. Electroanal. Chem.* **1977**, *84*, 1−20.
(61) Zeman, E. J.; Schatz, G. C. *J. Phys. Chem.* **1987**, *91*, 634−643. (b) Lyon, L. A.; Keating, C. D.; Fox, A. P.; Baker, B. E.; He, L.; Nicewarner, S. R.; Mulvaney, S. P.; Natan, M. J. *Anal. Chem.* **1998**, *70*, 341−362. (c) Moskovitz, M. *J. Chem. Phys.* **1982**, *77*, 4408−4416.
(62) Sanchez-Cortes, S.; Garcia-Ramos, J. V.; Morcillo, G. J. *J. Colloid Interface Sci.* **1994**, *167*, 428−436.
(63) (a) Wolkow, R. A.; Moskovits, M. *J. Chem. Phys.* **1992**, *96*, 3966−3980. (b) Gu, X. J.; Akers, K. L.; Moskovits, M. *J. Phys. Chem.* **1991**, *95*, 3696−3700.
(64) (a) Freeman, R. G.; Grabar, K. C.; Allison, K. J.; Bright, R. M.; Davis, J. A.; Guthrie, A. P.; Hommer, M. B.; Jackson, M. A.; Smith, P. C.; Walter, D. G.; Natan, M. J. *Science* **1995**, *267*, 1629−1632. (b) Chumanov, G.; Sokolov, K.; Gregory, B. W.; Cotton, T. M. *J. Phys. Chem.* **1995**, *99*, 9466−9471
(65) Baker, B. E.; Kline, M. J.; Treado, P. J.; Natan, M. J. *J. Phys. Chem. B* **1998**, *102*, 9404−9413.
(66) (a) Keating, C. D.; Kovaleski, K. M.; Natan, M. J. *J. Phys. Chem. B* **1998**, *102*, 9414−9425. (b) Keating, C. D.; Kovaleski, K. M.; Natan, M. J. *J. Phys. Chem. B* **1998**, *102*, 9414−9425.

Conclusion

Methodology to generate films composed of metal nanoparticles assembled in a stepwise fashion entirely from solution is presented; thus, there are few constraints on substrate size or shape. By controlling feature size, spacing, shape, and composition, the optical and electrical properties could be tuned. Films assembled using cross-linkers ≤8 Å in length have optical properties and conductivity comparable to their bulk metal counterpart. These were shown to be suitable for use as planar electrodes or SERS substrates. Au volume fractions were shown to be constant at all film heights, close to the critical volume fraction predicted by the scaling law for the metal−insulator transition. EFM reveals the presence of conductive and insulating regions consistent with the metal−insulator transition. Film roughness is believed to be responsible for the broad SPR curve observed from multilayer films on Au and glass and contribute to the SERS enhancement for BPE absorbed at Au or Ag nanoparticle assemblies. The fabrication of patterned multilayers with a low-error density using microcontact printing and construction of biologically active HRP-linked multilayers provide the groundwork for the development of colloidal nanoparticle devices as biosensors and electronics. Together, these results suggest that new materials design can begin on the nanoscale, especially when optical or electrical properties are to be considered.

Acknowledgment. Support from NSF (CHE-9256692, CHE-9627338), NIH (GM55312-01), and the Beckman Foundation is gratefully acknowledged. Acknowledgment is also made to the Electron Microscopy Facility for the Life Sciences in the Biotechnology Institute at The Pennsylvania State University.

Supporting Information Available: The following figures are availible as Supporting Information: Optical spectra of BSA-linked Au colloid multilayers and 2-mercaptoethanol linked Au and Ag multilayers; FE-SEM images of Au and Au/Ag nanoparticle multilayers; AFM line scans; EFM of Au multilayers as a function of voltage; cyclic voltammograms of Au colloid on SnO_2; SPR curve at 542.5 nm of Au colloid multilayers; SERS spectra of Au/Ag nanoparticle assemblies. This material is available free of charge via the Internet at http://pubs.acs.org.

CM990714C